Biosensors and Bioelectronics 131 (2019) 1–8

Contents lists available at ScienceDirect

Biosensors and Bioelectronics

journal homepage: www.elsevier.com/locate/bios

# Novel chitosan-Nafion composite for fabrication of highly sensitive impedimetric and colorimetric As(III) aptasensor

Sorour Salehi Baghbaderani, Abdollah Noorbakhsh*

*Department of Nanotechnology Engineering, Faculty of Advanced Sciences and Technologies, University of Isfahan, Isfahan 81746-73441, Iran*

ARTICLE INFO

*Keywords:*
Chitosan-Nafion
Arsenic detection
Electrochemicalaptasensor
Impedimetric
CNT-based amplification strategy

ABSTRACT

In the present work, for the first time we takes the advantages of chitosan-Nafion (Chit-Naf) composite as a highly conductive surface platform and a novel CNT-based signal amplification strategy to develop a lable-free impedimetricaptamer-based sensor for highly sensitive detection of As(III). The electrochemical impedance spectroscopy (EIS) investigations surprisingly revealed that the glassy carbon electrode (GC) electrode modified with Chit-Naf composite had higher electron transfer kinetics compared the bare GC, GC/Naf and GC/Chit electrodes, which promises a great potential as an efficient platform in construction of biosensing assays. In this work, we employed a signal amplification strategy based on carbon nanotube-bovine serum albumin (CNT-BSA) hybrid system, by which sensitivity and detection limit of the aptasensor for the detection of As(III) were obtained to be 100.82 $\Omega\,nM^{-1}$ and a of 74 pM, respectively. This protocol provided one of the lowest limits of detection for As(III) on aptamer-based electrodes recently described in the literature. Moreover, the change of the optical absorptive properties of CNTs upon biorecognition interactions provides a way to detect the biorecognition process and thus allowed us to design an optical As(III) aptasensor using the UV–Vis spectroscopic method. The discrimination capability of the fabricated aptasensor for recognizing As(III) in the presence of other metal ions and a complex matrix of waste water samples was successfully investigated. This protocol provided a new method for sensitive detection of As(III) with considerable advantages in terms of reproducibility, selectivity, being mediator free and regenerability of the sensing interface.

## 1. Introduction

Arsenic is considered as a toxic agent and known as carcinogenesis all around the world (Kim et al., 2009). Among the different four oxidation states of arsenic (-3, 0, +3, +5), arsenate [As(V)] and arsenite [As(III)] are the most common ions presented at natural water resources, and the toxicity of As(III) is 25–60 times higher than As(V) (Gao et al., 2013). Arsenic has negative effects on human health, and it has been shown to cause various diseases such as skin lesions, lung cancer, bladder cancer, liver cancer, and kidney disease (Gao et al., 2013; Weng et al., 2014). The World Health Organization (WHO) has estimated maximum permissible contamination level of 10 ppb for arsenic in drinking water (Gao et al., 2013; Moghimi et al., 2015). Therefore, introducing an analytical method with high sensitivity for the measurement of low levels of arsenic has been of great importance. In this context, aptamers offer excellent prospect as ideal recognition molecules to develop a new class of biosensors for the sensing of arsenic. Aptamers are recognized to be a new class of recognition molecules that can selectively bind to a wide range of targets from small molecules to large proteins and even whole cells and organisms (Iliuk et al., 2011). These molecules are single-stranded DNA or RNA oligonucleotides that can synthesize based on a combinatorial selection process named "systematic evolution of ligands by exponential enrichment (SELEX) (Ellington and Szostak, 1990). Besides the interesting recognition properties of aptamers for targeting a wide range of materials, some great advantages of this molecules, such as high stability (especially DNA aptamers), small size and easy of modification, may be highlighted, which make them suitable candidates as recognition elements for the construction of biosensing devices (Iliuk et al., 2011). In the past decade, aptamer-based sensing (aptasensing) of arsenic have attracted substantial research efforts, involving the application of various methods such as colorimetric (Gupta et al., 2016; Yang et al., 2017), chromatography (Keller et al., 2014; Lin et al., 2017), fluorescence (Ensafi et al., 2016), chemiluminescence (Lomonte et al., 2007), electrochemical techniques (Gao et al., 2013; Kempahanumakkagari et al., 2017; Moghimi et al., 2015; Yang et al., 2016), resonance Rayleigh scattering (Tang et al., 2014), atomic absorption spectrometry (AAS) (Wang et al., 2017), and inductively coupled plasma mass

* Corresponding author.
*E-mail addresses:* a.noorbakhsrezaei@ast.ui.ac.ir, noorbakhsh_a_sh@yahoo.com (A. Noorbakhsh).

https://doi.org/10.1016/j.bios.2019.01.059
Received 7 November 2018; Received in revised form 9 January 2019; Accepted 23 January 2019
Available online 05 February 2019
0956-5663/ 

spectrometry (ICPMS) (Gao et al., 2015). The electrochemical-based sensors have been attracting increased attention (Qin et al., 2017) thanks to their excellent advantages of high sensitivity and selectivity, low detection limit, the ability for miniaturization, simplicity, and low cost instrumentations (Zhang et al., 2018; Feng et al., 2014; Kempahanumakkagari et al., 2017). So, electrochemical aptamer-based sensors are considered to be attractive assays for the analysis of arsenic target, and the already reported results promise exciting future developments (Kempahanumakkagari et al., 2017).

In the present study, we introduced a chitosan-Nafion (Chit-Naf) interface for the first time and developed a highly sensitive and selective aptasensor for the detection of arsenic analyte based on aptamer-target biorecognition interactions. The optimized experimental conditions for achieving the best analytical signal of the aptasensor toward arsenic were evaluated. All fabrication steps of the aptasensor as well as its analytical performance toward the arsenic were investigated using electrochemical impedance spectroscopy (EIS) technique. For the first time in this study, we employed a novel amplification strategy based on $CNT_{COOH}$-BSA conjugate as a highly blocking system, by which its releasing from the electrode surface upon the biorecognition process would significantly increase the impedimetric response of the aptasensor to arsenic. The capability of the aptasensor for the regeneration of the sensing interface was examined. Also, the selective determination of arsenic in the presence of various interfering species and in the real samples was investigated in details.

## 2. Experimental section

### 2.1. Chemiclsl, apparatus, and measurements

All materials and reagents, apparatus and measurements are described in detail in the Supplementary file. The amine functionalized As (III) specific aptamer with the sequence of 5′-$C_6$-$NH_2$-ATGCAAACCCT TAAGAAAGTGGTCGTCCAAAAAACCATTG-3′ were purchased from Bioneer Co. The proposed As aptamer, introduced by Kim et al. (2009) previously, shows specific affinity to As(III) because of its unique structure (See Supplementary file for more information).

### 2.2. Preparation of Chit-Naf composite

Chit solution was prepared by ultrasonically dissolving of 10 mg Chit in 5 mL of 2% (v/v) acetic acid for 1 h. For obtaining 1% Nafion (Naf) solution, 0.2 mL of Naf solution (5%) was diluted with ethanol (99/9%). The Chit-Naf composite was prepared by simple mixing of Chit (2 mg/mL) and Naf (1%) solutions under vigorous stirring.

### 2.3. Preparation of $CNT_{COOH}$ and $CNT_{COOH}$-BSA

Carbon nanotubes (CNTs) were functionalized which carboxylic acid groups using a mixture of 3 M sulfuric acid and nitric acid (volume ratio of 3:1) for 10 h. The obtained functionalized CNTs ($CNT_{COOH}$) was washed several times with water until achieving neutral pH (pH = 7.0) and dried at room temperature.

To prepare $CNT_{COOH}$-BSA, bovine serum albumin (BSA) solution (1 mg/mL) was mixed with $CNT_{COOH}$ (1:1 wt ratio) under stirring for 24 h. The product was collected by centrifugation (10,000 rpm in Froilabo centrifuge for 10 min), washed two times with water and finally, dried at 50 °C in a regular oven.

### 2.4. Electrode modification

Glassy carbon (GC) electrode was subsequently polished with 1, 0.3 and 0.05 mm alumina slurry on the polishing pad, and then, ultrasonicated in an ethanol-distilled water bath for 5 min to remove the residual alumina particles. The Chit-Naf modified-GC (GC/Chit-Naf) electrode was fabricated by placing 2 μL of Chit-Naf composite on the surface of the GC electrode and drying at room temperature. The capture probe ($DNA_{cap}$) was immobilized on the electrode surface through glutaraldehyde cross-linking. For this purpose, 2 μL of glutaraldehyde (GLA) solution (5% v/w) was dropped onto the GC/Chit-Naf electrode surface for 45 min at room temperature, by which GLA linker was covalently attached to the GC/Chit-Naf surface through its reaction with amine groups of Chit. Then, 2 μL of 2 μM 5′-amine-DNA probe was incubated on the surface of the GC/Chit-Naf/GLA electrode for 1 h. As a result, $DNA_{cap}$ probe was covalently attached to the surface of the modified electrode through the reaction of -COH groups of GLA with $-NH_2$ groups of the $DNA_{cap}$ probe (Tahmasebi and Noorbakhsh, 2016). After that, BSA (0.05 mg/mL) was placed onto the GC/Chit-Naf/GLA/$DNA_{cap}$ electrode surface for 30 min to block the unreacted sites of the modified electrode. This electrode was labeled as the GC/Chit-Naf/GLA/$DNA_{cap}$/BSA electrode. Arsenic-specific aptamer (Apt probe) was attached to the electrode surface through its hybridization with the $DNA_{cap}$ probe sequence as a result of dropping 2 μL of 3′-amine-Apt probe (5 μM) on the GC/Chit-Naf/GLA/$DNA_{cap}$/BSA electrode surface for 2 h. In the last step, to provide a means of signal amplification path in the detection of As(III), 2 μL $CNT_{COOH}$-BSA nanocomposite was incubated on the electrode surface for 60 min, in which $CNT_{COOH}$-BSA was attached to the Apt probe through glutaraldehyde cross-linking. This electrode was denoted as GC/Chit-Naf/GLA/$DNA_{cap}$/BSA/Apt/GLA/$CNT_{COOH}$-BSA electrode. Each steps of electrode modification were followed using EIS method.

For the determination of As(III), GC/Chit-Naf/GLA/$DNA_{cap}$/BSA/Apt and GC/Chit-Naf/GLA/$DNA_{cap}$/BSA/Apt/GLA/$CNT_{COOH}$-BSA electrodes were exposed to a series of different As(III) concentrations for 45 min and the aptasensor response in the absence and presence of target was investigated by EIS technique in 0.1 M KCl solution containing 10 mM $Fe(CN)_6^{3-/4-}$. At all steps, the modified electrodes were carefully rinsed with phosphate-potassium chloride-sodium chloride buffer solution and distilled water to remove non-binding and weakly binding materials. EIS and UV–Vis spectrophotometric methods were used to investigate As(III) detection. Experimental parameters used in all steps of electrode modification and for As(III) determination, including Chit to Naf ratio, the $DNA_{cap}$-Apt hybridization time, aptamer concentration, incubation time of As(III) and washing time of the electrode after incubation of $DNA_{cap}$ and Apt probes, were in their optimum values.

## 3. Results and discussion

### 3.1. Characterization of the Chit-Naf composite and electrode platform

In the present work, we introduced Chit-Naf composite as a novel substrate for application in biosensing assays, which offered surprisingly great potential for construction of the presented analytical device. The synthesized Chit-Naf composite was investigated by EIS, cyclic voltammetry (CV), Fourier transform infrared (FTIR) spectroscopy techniques and Field emission scanning electron microscopy (SEM). In an attempt to investigate the electron transfer properties of the Chit-Naf composite, we compared the EIS spectra obtained on Chit-Naf modified glassy carbon (GC/Chit-Naf) electrode with those of GC, GC/Chit and GC/Naf electrodes (Fig. 1A). The charge transfer resistance ($R_{ct}$) is proportional to the semicircle diameter in the Nyquist diagram, and more exactly it can be obtained by appropriate fitting of the EIS data to an appropriate model. From the Fig. 1A, it can be seen that compared to the bare GC electrode (plot a), there was an observed lower value of $R_{ct}$ for the GC/Chit electrode (plot b) that is attributed to the electrostatic attraction between positively charged amine groups of Chit and negatively charged $[Fe(CN)_6]^{3-/4-}$ redox system. For the GC/Naf electrode (plot c), $R_{ct}$ increased significantly compared to the bare GC electrode because of the blocking effect of Naf as well as the electrostatic repulsion interactions between negatively charged sulfonate groups of Naf and $[Fe(CN)_6]^{3-/4-}$ redox probe (Chen et al., 2007; Zarei and Khodadadi,

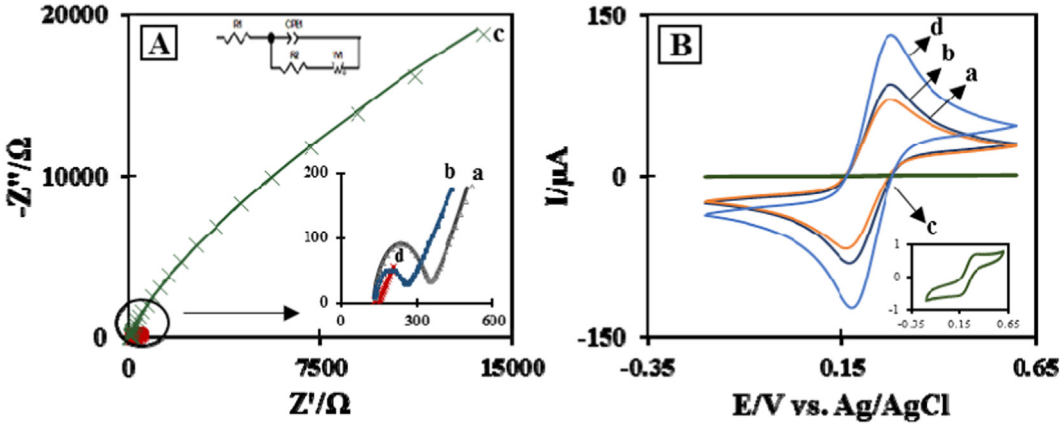


**Fig. 1.** (A) EIS complex plane plots and (B) CVs of (a) GC, (b) GC/Chit, (c) GC/Naf and (d) GC/Chit-Naf electrodes obtained in 0.1 M KCl electrolyte solution containing 10 mM $Fe(CN)_6^{-3/-4}$. Scan rate: 60 mV $s^{-1}$ EIS plots were recorded at an applied potential of 0.22 V and a frequency range of 0.1–10 kHz. Symbols and trend lines respectively show the experimental and the fitted data based on modified Randle's model shown in the inset of Fig. A. See Table S1 for further information.

2017). Surprisingly, the value of $R_{ct}$ of the GC electrode decreased dramatically after modifying with Chit-Naf composite. This result is interesting since the electron transfer rate at the GC/Chit-Naf electrode is faster than that obtained at GC, and even GC/Chit electrode (Table S1). The same results were observed from CV measurements. As can be seen in Fig. 1B, GC/Chit-Naf electrode has the highest anodic and cathodic peak current and lowest peak-to-peak separation. The observed decrease in $R_{ct}$ of the GC/Chit-Naf electrode may be originated from the possible interactions between adjacent groups of Chit and Naf that leads to an ionically cross-linked network, as shown in Fig. S2, which can accelerate ion (proton) transfer in electrochemical systems From FT-IR studies of Chi, Naf and Chit-Naf film, (discussed in the Supplementary file; Section S2 and Fig. S1) the observed shift in absorption band of Chi and Naf moiety in the Chit-Naf film, and the decrease in $R_{ct}$ observed on GC/Chit-Naf electrode may be originated from the possible interactions between adjacent groups of chitosan and Nafion. These interactions can be led to an ionically cross-linked network, as shown in Fig. S2, which can accelerate ion (proton) transfer in electrochemical systems. The acide–base interaction between the amino groups of chitosan and sulfonic acid groups of Nafion can be described by the possible mechanism as follows (Eq. (1)):

$$Naf\text{–}SO_3H + Chit\text{–}NH_2 \rightarrow [Naf\text{–}SO3]^{-}{}^{+}[ChitNH\text{–}H_2] \quad (1)$$

Same studies on the interaction of different types of acid–base blend membranes containing sulfonate and amine groups, reported by Kerres et al. (2000) and Kerres (2001), have indicated that a flexible ionomer networks can be formed by proton-transfer from the polymeric acid onto the polymeric base. Some other studies are presented on the Nafion interaction with acidic polymers such as poly (vinyl pyrrolidone) (PVP) (Li et al., 2010) and polypyrrole composite (Park et al., 2006). However, there are no reported studies so far in the literature on the Chit-Naf interaction. Fig. S3 shows the FE-SEM images of Chi-Naf composite in different magnifications. As can be seen, Chi-Naf composite can be formed in a very homogeneous film on the electrode surface, with makes it a very suitable material for modification of electrode surfaces.

The experimental results obtained in the present study (Supplementary file; Section S3, Fig. S4 and Table S2) demonstrated that in comparison with Chi film, Chit-Naf composite could generate an appropriate platform for immobilization of amine functionalized DNA probes in order to fabricate a very sensitive aptasensor.

The various steps of fabrication of the aptasensor on the Chit-Naf substrate are shown in Fig. 2A. Nyquist plots obtained on GC, GC/Chit-Naf, GC/Chit-Naf/GLA, GC/Chit-Naf/GLA/$DNA_{cap}$, GC/Chit-Naf/GLA/$DNA_{cap}$/BSA, and GC/Chit-Naf/GLA/$DNA_{cap}$/BSA/Apt electrodes are presented in Fig. 2B and the quantitative values of the kinetic parameters ($R_{ct}$, $R_{s,}$ and n) extracted from the approximation of the EIS diagrams are given in Table S3. Starting from the bare GC electrode (plot a), the value of $R_{ct}$ decreased upon the immobilization of Chit-Naf film (plot b) and increased by the sequential assembling of the layers GLA, $DNA_{cap}$ probe, BSA and Apt probe (plots e-f, respectively) on the surface. These results verified the immobilization of $DNA_{cap}$ probe on the electrode surface and its hybridization with the Apt probe. Furthermore, the immobilization of $DNA_{cap}$ and Apt probes on the surface was verified by EDAX experiments. Fig. 2C shows the EDAX spectra of Chit-Naf and Chit-Naf/GLA/$DNA_{cap}$/Apt-modified electrodes. The elements of C, N, O, F and S can be seen in the GC/Chit-Naf spectra, showing the coupling of Chit-Naf film with the surface. For the EDAX spectra of the GC/Chit-Naf/GLA/$DNA_{cap}$/Apt electrode, the presence of phosphorus elements confirmed the immobilization of $DNA_{cap}$ and Apt probes on the surface of Chit-Naf film. The obtained results are in good agreement with other previous works (Tabasi et al., 2017). From the above results, compared to the Chit, the Chit-Naf substrate is very successful in immobilization and hybridization of DNA strands on the surface and has a substantial role in designing the aptasensor.

### 3.2. Analytical performance of the As(III) aptasensor

In the present work, in order to improve the analytical performance of the aptasensor for detection of As(III), experimental parameters, such as Chit to Naf ratio, the $DNA_{cap}$-Apt hybridization time, aptamer concentration, and incubation time of As(III) were investigated and optimized (Supplementary file; section S4, Fig. S5 and Fig. S6).

For analytical detection of As(III), the fabricated aptasensor was incubated in various concentrations of As(III). Fig. 3A depicts schematically the impedimetric analysis of As(III) by the present aptasensor. Owing to the fact that the As(III)-aptamer complex is more stable than the aptamer-DNA hybrid (Cui et al., 2016; Song et al., 2016), As(III) induced the dissociation of aptamer molecules from the sensing interface to form the aptamer-As(III) complex, which led to the facilitation of the electron transfer processes from or to the surface. The charge transfer resistance change ($\Delta R_{ct}$) of the GC/Chit-Naf/GLA/$DNA_{cap}$/BSA/Apt electrode in the absence ($R_{ct(a)}$) and presence ($R_{ct(b)}$) of As(III) was considered as the aptasensor response (Supplementary file, Fig. S7). Fig. 3B shows the EIS responses of the aptasensor to different concentrations of As(III) within the range of 1–2000 nM under the optimized conditions. As the As(III) concentration was increased, the $R_{ct}$ value decreased accordingly. The aptasensor response was found to produce a linear relation over two concentration ranges of 1–50 nM, and 100–500 nM (according to Eqs. (2) and (3)):

$$R_{ct}(\Omega) = 5.301[As(III)]\,(nM) + 11.97(\Omega) \qquad R^2 = 0.9982 \quad (2)$$

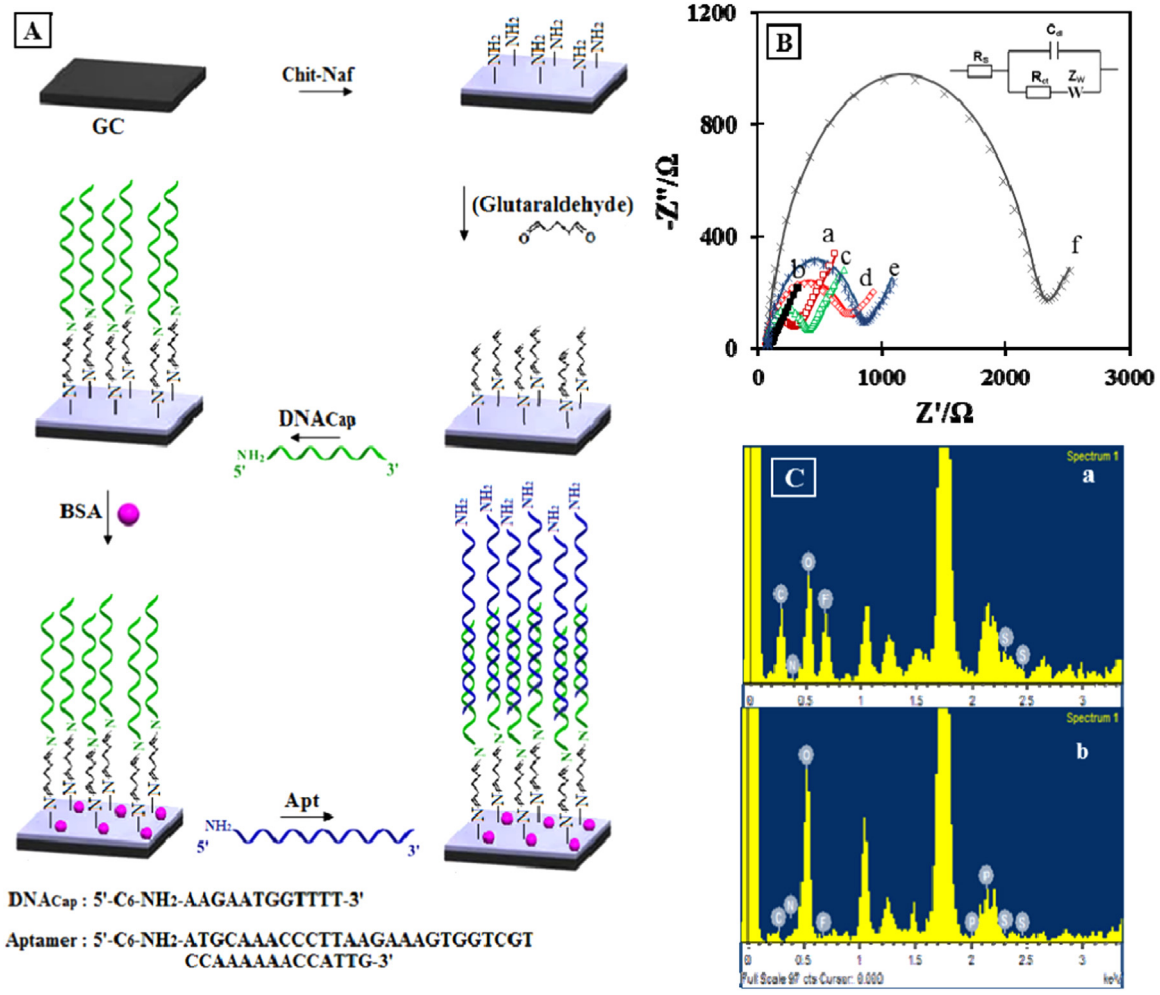


**Fig. 2.** (A) Schematic representation of the aptasensor fabrication steps, (B) EIS complex plane plots obtained on (a) GC, (b) GC/Chit-Naf, (c) GC/Chit-Naf/GLA, (d) GC/Chit-Naf/GLA/$DNA_{cap}$, (e) GC/Chit-Naf/GLA/$DNA_{cap}$/BSA and (f) GC/Chit-Naf/GLA/$DNA_{cap}$/BSA/Apt electrodes, (C) EDAX spectra of the GC/Chit-Naf/GLA/$DNA_{cap}$/Apt electrode. EIS data were recorded and approximated in the same conditions as (Fig. 1). See Table S3 for kinetic parameters extracted from approximation of the EIS diagrams.

$$R_{ct}(\Omega) = 1.18[As(III)]\,(nM) + 244.09(\Omega) \qquad R^2 = 0.9902 \qquad (3)$$

From the linear calibration curve in the range of 1–50 nM (Eq. (2)), the limit of detection ((S/N = 3)) and the sensitivity of the aptasensor for detection of As(III) were calculated to be 0.78 nM and 5.30 $\Omega\,nM^{-1}$, respectively. The present aptasensor demonstrated a desirable analytical performance compared to the recently reported As(III) aptasensors that some of them are presented in Table 1. An important feature for a sensor is its reproducibility and so, this parameter was evaluated by calculating the relative standard deviation (RSD) of three aptasensors used for the detection of 250 nM As(III)). The value of RSD was found to be 6.6%, indicating the acceptable reproducibility of the aptasensor that can be related to the stability of Chit-Naf substrate for immobilization of $DNA_{cap}$ and Apt sequences and high binding affinity of aptamer to As(III). Moreover, the GC/Chit-Naf/GLA/$DNA_{cap}$/BSA/Apt sensor can be simply regenerated by reconstitution of aptamer probe on the sensing interface, as is discussed in details in Supplementary file (Section S5 and Fig. S8).

### 3.3. Signal amplification system

In order to amplify the analytical signal of As(III), we developed a simple signal amplification strategy by the use of a nanobioconjugated system based on bovine serum albumin (BSA) and carbon nanotube (CNT). The integration of BSA, a well-known high-molecular-weight protein (Ojha and Das, 2010; Tripathi et al., 2006), into high-surface-area $CNT_{COOH}$ (Yang et al., 2015), could yield new $CNT_{COOH}$-BSA hybrid system with synergetic properties and functions. The $CNT_{COOH}$-BSA conjugated system was prepared via carbodiimide coupling of the carboxylic groups of activated CNT ($CNT_{COOH}$) to the amino groups of BSA molecules, and then it was investigated using EIS, CV, AFM, dynamic light scattering (DLS), zeta potential and FT-IR analysis, which are presented in Supplementary file in details (Section S6, Figs. S9 to S12). AFM (Fig. S9), EIS and CV (Fig. S10), DLS (Fig. S11), and FT-IR analysis (Fig. S13) demonstrated the successful formation of the $CNT_{COOH}$-BSA conjugate system. Also, zeta potential analysis shows the good dispersibility of $CNT_{COOH}$-BSA nanostructures at physiological pH (Fig. S12). From the EIS results (Fig. S10A), $R_{ct}$ value for $CNT_{COOH}$-BSA film was found to be higher than those obtained for $CNT_{COOH}$ and BSA, which can be attributed to the large surface area of $CNT_{COOH}$ covered by the BSA big protein. Since the analytical strategy studied in this work is based on the $R_{ct}$ changes ($\Delta R_{ct}$) of the aptasensor during the sensing process, the attachment of $CNT_{COOH}$-BSA whit highly blocking effect to the sensing interface can provide an effective means to amplify the variations of $R_{ct}$ that occur at surface upon the biorecognition events. Fig. 4A depicts schematically the amplified EIS analysis of As(III) by the use of $CNT_{COOH}$-BSA system. The $CNT_{COOH}$-BSA system was covalently attached to the GC/Chit-Naf/GLA/$DNA_{cap}$/BSA/Apt electrode surface via cross-linking of amine groups of BSA with amino-functionalized aptamer probe through the glutaraldehyde cross-linker,

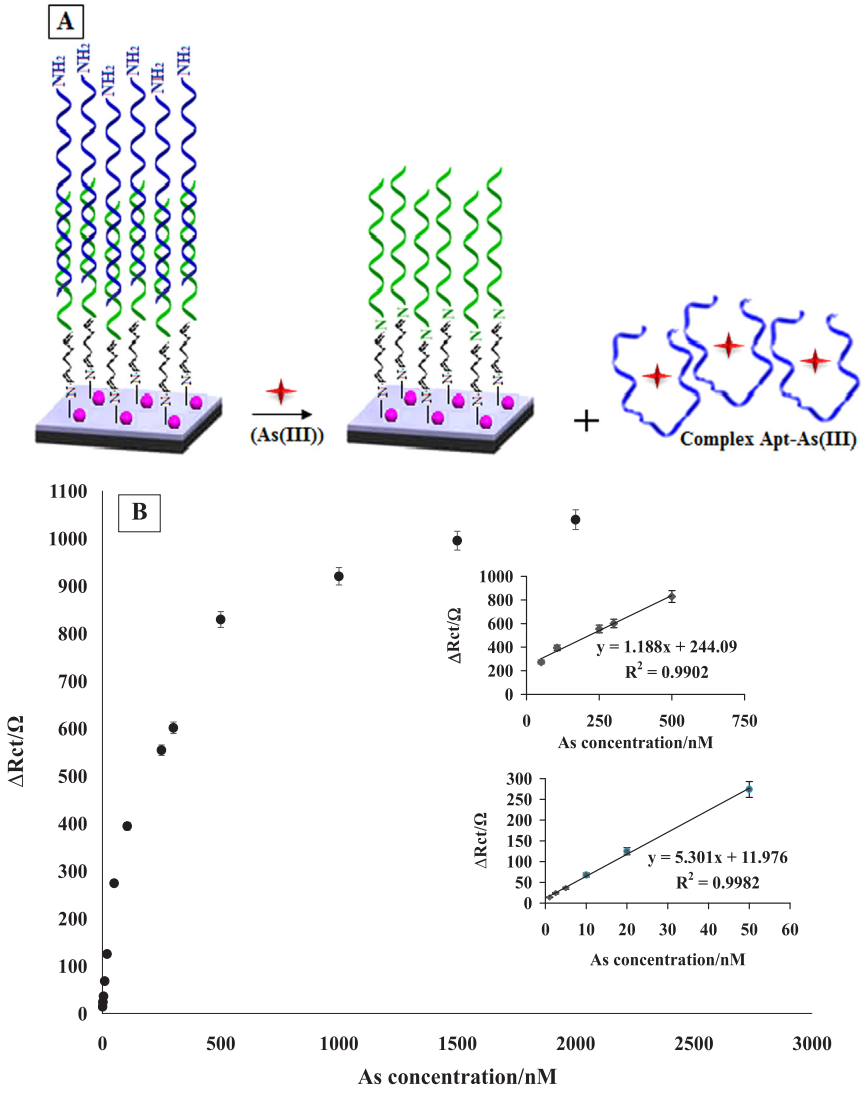


**Fig. 3.** (A) Schematic representation of the the impedimetric analysis of As(III) by the present aptasensor. (B) The calibration graph for As(III) detection by GC/Chit-Naf/GLA/DNAcap/BSA/Apt electrode (The EIS responses of the aptasensor to different concentrations of As(III) within the range of 1 nM to 2000 nM under the optimized conditions).

**Table 1**
Comparison of the analytical data of various As(III) aptasensors.

| Method | LOD (nM) | Linear range (nM) | Ref |
|---|---|---|---|
| Colorimetric aptasensor | 79.8 | 665–931 | (Divsar et al., 2015) |
| Surface Enhanced Raman Scattering | 1.33 | 6.65–133 | (Song et al., 2016) |
| Fluorescent aptasensor | 0.07 | 0.13–0.13 × $10^6$ | (Pan et al., 2018) |
| Fluorescent aptasensor | 0.45 | 2–500 | (Taghdisi et al., 2018) |
| Fluorescent aptasensor | 11.97 | 53.2–798 | (Oroval et al., 2017) |
| Electrochemiluminescence | 8.25 | 13.3–665 | (Liang et al., 2018) |
| Electrochemical aptasensor | 0.27 | 1.33–2.7 × $10^3$ | (Gu et al., 2018) |
| Electrochemical aptasensor | 6.65 | 6.65–133 | (Wang et al., 2015) |
| Electrochemical aptasensor | 0.15 | 0.2–100 | (Cui et al., 2016) |
| Electrochemical aptasensor | 0.001 | 1.33–2660 | (Wen et al., 2017) |
| Electrochemical aptasensor | 0.77 | 2.66–6650 | (Wen et al., 2018) |
| Electrochemical aptasensor | 0.007 | 0.01–10 | (Zhang et al., 2017) |
| Electrochemical aptasensor | 18.6 × $10^{-7}$ | (0.05–40) × $10^{-4}$ | (Ensafi et al., 2018) |
| Electrochemical aptasensor | 800 | 0.05–10 ppm | (Vega-Figueroa et al., 2018) |
| Electrochemical aptasensor | 0.78 | 1–50, 100–500 | This work |
| Electrochemical aptasensor with signal amplification | 0.074 | 0.15–10, 20–100 | This work |
| Optical aptasensor with signal amplification | 6.1 | 10–50 | This work |

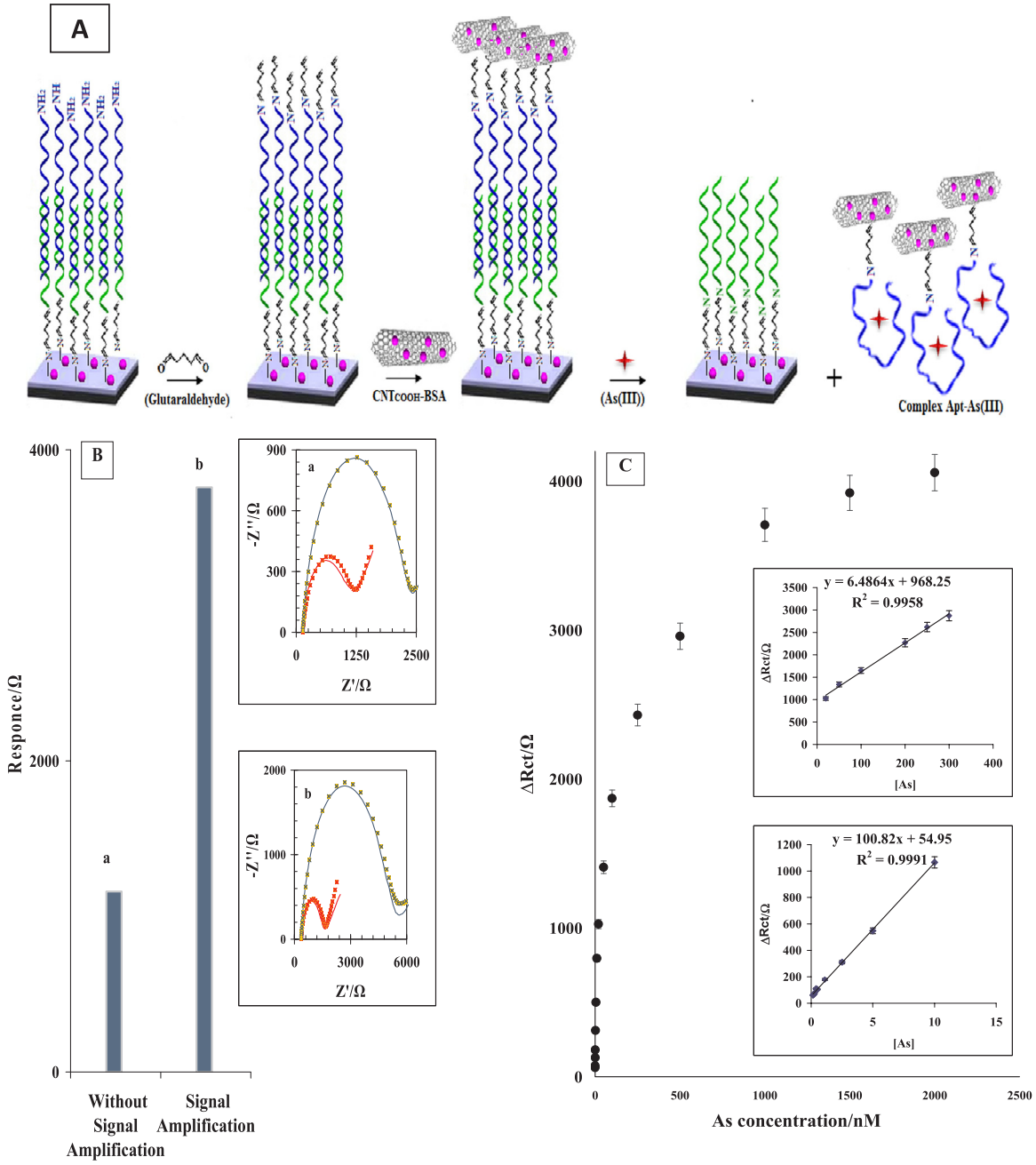


**Fig. 4.** (A) Schematic representation of the various amplification steps of the aptasensor in the presence of $CNT_{COOH}$-BSA hybrid system; (B) analytical signal of the aptasensor in EIS in the absence (a) and presence (b) of amplification system; (C) calibration graph for impedimetric detection of As(III) on the amplified aptasensor in various concentration range of 150 pM–2000 nM.

which resulted in an increase in the $R_{ct}$ value from 2210 Ω to 4950 Ω, observed from the EIS measurements (Fig. 4B). As is shown in Fig. 4B, the EIS response of the aptasensor to 1000 nM As(III) was increased from 920 Ω to 3706 Ω by the use of this amplification system. The variation in the $R_{ct}$ value ($\Delta R_{ct}$) in EIS plots of the GC/Chit-Naf/GLA/$DNA_{cap}$/BSA/Apt/$CNT_{COOH}$-BSA electrode was analyzed as a function of As(III) concentration in the range of 150 pM to 2000 nM (Supplementary file, Fig. S14), and a calibration graph was obtained (Fig. 4C). The response was found to be linear over the concentration ranges of 0.15–10 nM and 20–250 nM As(III). By using the amplification strategy used in this work, the analytical performance of the aptasensor for the detection of As(III) was significantly improved, achieving a sensitivity of 100.82 Ω $nM^{-1}$ and a limit of detection of 74 pM. This strategy led to about 11- and 19-fold improvement in detection limit and sensitivity, respectively, which represented one of the lowest limits of detection for As(III) on aptamer-based electrodes currently described in the literature (see Table 1).

### 3.4. UV–Vis detection of As(III)

Since the CNTs have a high absorptive ability in UV–Vis region (Huang et al., 2013), the GC/Chit-Naf/GLA/$DNA_{cap}$/BSA/Apt/$CNT_{COOH}$-BSA modified electrode can be employed as an optical aptasensor for detection of As(III) using the UV–Vis spectroscopic method. From the UV–Vis spectrum of Chit-Naf/GLA/$DNA_{cap}$/BSA/Apt/$CNT_{COOH}$-BSA-modified quartz substrate shown in Fig. 5A, a strong peak at 255 nm caused by the absorption of $CNT_{COOH}$ was observed. The presence of As(III) led to an obvious decrease in the peak intensity,

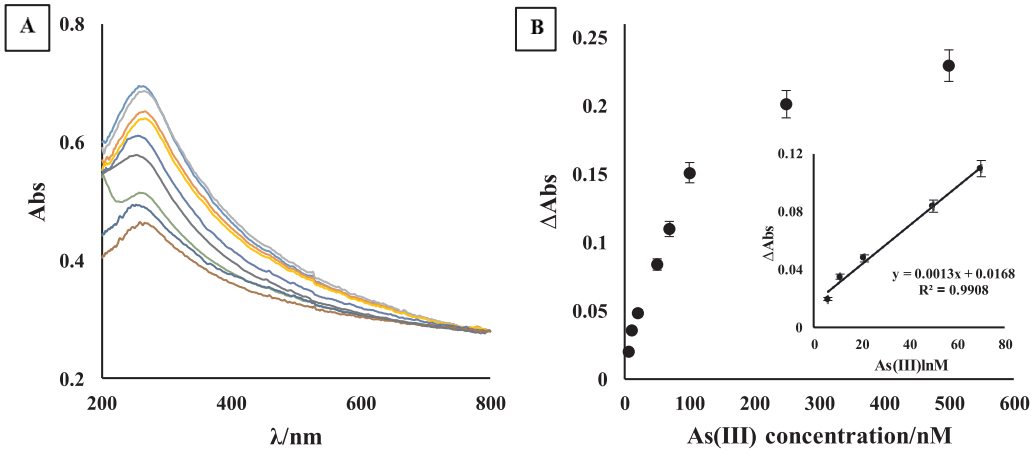


**Fig. 5.** (A) UV–Vis spectrum of Chit-Naf/GLA/$DNA_{cap}$/BSA/Apt/$CNT_{COOH}$-BSA-modified exposed to a series of different As(III) concentrations (10–500 nM) and (B) the related calibration curve for As(III) detection.

which is attributed to the detachment of Apt/$CNT_{COOH}$-BSA from the surface upon the binding of aptamer and As(III). The absorbance intensity of CNTs peak decreased with increasing of As(III) amount in the concentration ranges of 10–500 nM and a calibration curve was achieved (Fig. 5B). The optical response of the aptasensor was found to be linear over the concentration of 10–50 nM As(III). The detection limit and sensitivity of optical aptasensor were calculated to be 6.1 nM and 0.0013 $nM^{-1}$, respectively.

### 3.5. Selectivity of the aptasensor

To demonstrate the selectivity of the aptasensor for detection of As (III), the analytical signal of the GC/Chit-Naf/GLA/$DNA_{cap}$/BSA/Apt electrode in EIS was compared for 1 μM As(III) and 100 μM of various metal ions, including Fe(III), Ca(II), Ni(II), Co(II), Cu(II), Zn(II), Pb(II), Hg(II), Na(I) and As(V). As shown in Fig. S15, except for As(V), no significant response were observed for other interfering metal ions even though their concentrations were 100 times higher than the concentration of As(III), indicating the excellent selectivity of the aptasensor for As(III). These control experiments, however, revealed a weak affinity of As(V) for the aptamer used in this work. The results showed that the aptasensor developed in this study has high binding affinity to As(III) compared to other ions, which make it as a highly selective aptasensor for determination of As(III).

### 3.6. Determination of As(III) in the real samples

We evaluated the applicability of the designed aptasensor by the detection of As(III) in real samples, including drinking water of our university and industrial wastewater of our city. To remove the particulate solids from the samples, they were first filtered through a 0.2 μm membrane. Then, As(III) solution with two concentrations of 10 and 100 nM As(III) were prepared both in standard solution and two real samples and analyzed using the proposed sensor. Table S4 shows the results of analysis samples, representing fairly good recovery values in the range of 92.36–118.50% for the spiked As(III). Also, hydride generation- atomic absorption spectroscopy (HG-AAS) method was applied to confirm the presented As(III) sensing system. The results showed good agreement between two methods for detection of As(III) in real samples. Therefore, the designed aptasensor can detect As(III) in real samples.

## 4. Conclusion

In this study, a novel Chit-Naf composite were introduced and characterized. Also, a very sensitive impedimetric aptamer-based biosensor was developed for highly sensitive detection of As(III) as a model. The investigations indicated the facilitated electron transfer kinetics at the GC/Chit-Naf electrode compared to the bare GC, GC/Naf and, GC/Chit electrodes, making Chit- Naf as an ideal platform for biosensor applications. In this work, $CNT_{COOH}$-BSA system was used for signal amplification of proposed AS(III) aptasensor. By employing this signal amplification strategy, sensitivity and detection limit of the aptasensor for the detection of As(III) were obtained to be 100.82 Ω $nM^{-1}$ and 74 pM. The high affinity of As(III)-specific aptamer as the recognition layer to As(III) resulted in a highly selective aptasensor for recognizing of As(III) in the complex matrix of waste water samples with grate accuracy. The electrochemical studies illustrated the reproducible and regenerative characteristics of the prepared sensing interface, which can be used for subsequent determination of As(III). Also, experimental results demonstrated the application of proposed Chi-Naf and $CNT_{COOH}$-BSA nanobioconjugated system for fabrication of the sensitive colorimetric aptasensors.

## Acknowledgements

This work was financially (Grant ID: 14459/93) supported by the University of Isfahan, Iran. The authors thank Dr. Ensiyeh Sharifi for her valuable discussion.

## Declaration of interests

The authors declare that they have no known competing financial interests or personal relationships that could have appeared to influence the work reported in this paper.

## Appendix A. Supporting information

Supplementary data associated with this article can be found in the online version at doi:10.1016/j.bios.2019.01.059.

## References

Chen, H., Wang, Y., Liu, Y., Wang, Y., Qi, L., Dong, S., 2007. Electrochem. Commun. 9, 469–474.
Cui, L., Wu, J., Ju, H., 2016. Biosens. Bioelectron. 79, 861–865.
Divsar, F., Habibzadeh, K., Shariati, S., Shahriarinour, M., 2015. Anal. Methods 7, 4568–4576.
Ellington, A.D., Szostak, J.W., 1990. Nature 346, 818.
Ensafi, A.A., Akbarian, F., Heydari-Soureshjani, E., Rezaei, B., 2018. Biosens. Bioelectron. 122, 25–31.
Ensafi, A.A., Kazemifard, N., Rezaei, B., 2016. Biosens. Bioelectron. 77, 499–504.
Feng, L., Gao, G., Zahang, C., Ma, J., Cui, D., 2014. J. Exp. Nanosci. 9, 452–462.
Gao, C., Yu, X.-Y., Xiong, S.-Q., Liu, J.-H., Huang, X.-J., 2013. Anal. Chem. 85,

2673–2680.
Gao, Y., Sturgeon, R.E., Mester, Z., Hou, X., Yang, L., 2015. Anal. Chim. Acta 901, 34–40.
Gu, H., Yang, Y., Chen, F., Liu, T., Jin, J., Pan, Y., Miao, P., 2018. Chem. Eng. J. 353, 305–310.
Gupta, A., Verma, N.C., Khan, S., Nandi, C.K., 2016. Biosens. Bioelectron. 81, 465–472.
Huang, J.-H., Hong, Y.-J., Chang, Y.-T., Chang, P., Yew, T.-R., 2013. J. Mater. Chem. B 1, 5389–5392.
Iliuk, A.B., Hu, L., Tao, W.A., 2011. Anal. Chem. 83, 4440–4452.
Keller, N.S., Stefánsson, A., Sigfússon, B., 2014. Talanta 128, 466–472.
Kempahanumakkagari, S., Deep, A., Kim, K.-H., Kailasa, S.K., Yoon, H.-O., 2017. Biosens. Bioelectron. 95, 106–116.
Kerres, J., Ullrich, A., Häring, T., Baldauf, M., Gebhardt, U., Preidel, W., 2000. J. New Mater. Electrochem. Syst. 3, 129–239.
Kerres, J.A., 2001. J. Membr. Sci. 185, 3–27.
Kim, M., Um, H.-J., Bang, S., Lee, S.-H., Oh, S.-J., Han, J.-H., Kim, K.-W., Min, J., Kim, Y.-H., 2009. Environ. Sci. Technol. 43, 9335–9340.
Li, T., Zhong, G., Fu, R., Yang, Y., 2010. J. Membr. Sci. 354, 189–197.
Liang, R.-P., Yu, L.-D., Tong, Y.-J., Wen, S.-H., Cao, S.-P., Qiu, J.-D., 2018. Chem. Commun. 54, 14001–14004.
Lin, C.-H., Chen, Y., Su, Y.-A., Luo, Y.-T., Shih, T.-T., Sun, Y.-C., 2017. Anal. Chem.
Lomonte, C., Currell, M., Morrison, R.J., McKelvie, I.D., Kolev, S.D., 2007. Anal. Chim. Acta 583, 72–77.
Moghimi, N., Mohapatra, M., Leung, K.T., 2015. Anal. Chem. 87, 5546–5552.
Ojha, B., Das, G., 2010. J. Phys. Chem. B 114, 3979–3986.
Oroval, M., Coll, C., Bernardos, A., Marcos, M.D., Martinez-Manez, R., Shchukin, D.G., Sancenón, F., 2017. ACS Appl. Mater. Interfaces 9, 11332–11336.
Pan, J., Li, Q., Zhou, D., Chen, J., 2018. Talanta 189, 370–376.
Park, H.S., Kim, Y.J., Hong, W.H., Lee, H.K., 2006. J. Membr. Sci. 272, 28–36.
Qin, W., Wang, K., Xia, K., Hou, Y., Lu, W., Xu, H., Wo, Y., Feng, S., Cui, D., 2017. Biosens. Bioelectron. 90, 508–515.
Song, L., Mao, K., Zhou, X., Hu, J., 2016. Talanta 146, 285–290.
Tabasi, A., Noorbakhsh, A., Sharifi, E., 2017. Biosens. Bioelectron. 95, 117–123.
Taghdisi, S.M., Danesh, N.M., Ramezani, M., Emrani, A.S., Abnous, K., 2018. Sens. Actuators B. Chem. 256, 472–478.
Tahmasebi, F., Noorbakhsh, A., 2016. Electroanalysis 28, 1134–1145.
Tang, M., Wen, G., Liang, A., Jiang, Z., 2014. Luminescence 29, 603–608.
Tripathi, V.S., Kandimalla, V.B., Ju, H., 2006. Biosens. Bioelectron. 21, 1529–1535.
Vega-Figueroa, K., Santillán, J., Ortiz-Gómez, V., Ortiz-Quiles, E.O., Quiñones-Colón, B.A., Castilla-Casadiego, D.A., Almodóvar, J., Bayro, M.J., Rodríguez-Martínez, J.A., Nicolau, E, 2018. Aptamer-Based Impedimetric Assay of Arsenite in Water: Interfacial Properties and Performance. ACS Omega 3 (2), 1437–1444.
Wang, Q., Yu, Z., Lan, J., Liu, A., Tian, Y., 2017. Microchem. J. 133, 412–416.
Wang, Y., Wang, P., Wang, Y., He, X., Wang, K., 2015. Talanta 141, 122–127.
Wen, S.-H., Wang, Y., Yuan, Y.-H., Liang, R.-P., Qiu, J.-D., 2018. Anal. Chim. Acta 1002, 82–89.
Wen, S., Zhang, C., Liang, R., Chi, B., Yuan, Y., Qiu, J., 2017. Microchim. Acta 184, 4047–4054.
Weng, C.-I., Cang, J.-S., Chang, J.-Y., Hsiung, T.-M., Unnikrishnan, B., Hung, Y.-L., Tseng, Y.-T., Li, Y.-J., Shen, Y.-W., Huang, C.-C., 2014. Anal. Chem. 86, 3167–3173.
Yang, M., Chen, X., Jiang, T.-J., Guo, Z., Liu, J.-H., Huang, X.-J., 2016. Anal. Chem. 88, 9720–9728.
Yang, N., Chen, X., Ren, T., Zhang, P., Yang, D., 2015. Sens. Actuators B Chem. 207, 690–715.
Yang, T., Zhang, X.-X., Yang, J.-Y., Wang, Y.-T., Chen, M.-L., 2017. Talanta 177, 212–216.
Zarei, K., Khodadadi, A., 2017. Ecotoxicol. Environ. Saf. 144, 171–177.
Zhang, A., Guo, W., Ke, H., Zhang, X., Zhang, H., Huang, C., Yang, D., Jia, N., Cui, D., 2018. Biosens. Bioelectron. 101, 219–226.
Zhang, Z., Ji, H., Song, Y., Zhang, S., Wang, M., Jia, C., Tian, J.-Y., He, L., Zhang, X., Liu, C.-S., 2017. Biosens. Bioelectron. 94, 358–364.